Anisotropic Magnetism and Magnetoresistance in Iron Nanowire Arrays

M. N. Ou,[1,2] T. J. Yang,[2] and Y. Y. Chen[1]

[1] *Institute of Physics, Academia Sinica, Taipei, Taiwan, R.O.C.*

[2] *Department of Electrophysics, National Chiao Tung University, Hsinchu, Taiwan, R.O.C.*

(Received September 4, 2008)

Highly ordered ferromagnetic iron nanowire (Fe NW) arrays with diameters of about 60 nm and 200 nm were fabricated by electro-chemical deposition into anodic aluminum oxide (AAO) templates. The magnetization measurements show the 60 nm NWs as having a larger anisotropic magnetization. This result was illustrated by the magnetic easy axis and preferred crystal orientation of [110] along with the longitudinal direction of the NWs, revealed by the X-ray diffraction (XRD) patterns. The obtained quadratic magnetic field dependence of the normalized magnetoresistance (MR) at low field for both 60 and 200 nm NWs is attributed to the anisotropic magnetoresistance in low-dimensional systems. Furthermore, the enhanced MR observed in the 60 nm NWs is attributed to additional spin-diffusion mechanisms.

PACS numbers: 62.23.Hj, 73.43.Qt, 75.30.Gw

I. INTRODUCTION

Due to the high density of electronic states, the diameter dependence of the band gap, the enhanced surface scattering of electrons and phonons, the large surface to volume ratio, and the large aspect ratio, nanowires (NWs) of metals and semiconductor, exhibiting very different behavior from those of the bulk materials, have attracted intensive interest from researchers for the past decades. In particular, the ferromagnetic NW arrays were paid more attention in recent years, due to their great potential for applications in high-density magnetic storage media, high-sensitivity magnetic sensors, and biological technology [1–4]. The application of perpendicular magnetic recording (PMR) to the NW arrays is potentially capable of overcoming the thermal stability limit of superparamagnetism for modern magnetic storage devices with bit densities in excess of 100 Gbit in^{-2} [5–7]. Thus, in addition to the fabrication of magnetic NW arrays with proper aspect ratio, the understanding of their magnetic and electrical transport properties becomes more interesting and useful for applications.

A porous anodic aluminum oxide (AAO) template is considered to be a potential material for nanowire fabrication because of its high-density and uniformity of pores. Although the fabrication of Fe NW arrays and their magnetic properties have been widely studied [8–12], works on the magneto transport properties were seldom reported. In this work we present the results of our studies on the magnetism and magneto transport properties in Fe NW arrays.

II. SYNTHESIS OF NANOWIRE ARRAYS

Several techniques have been used to synthesize high-density and regular nano-pore arrays, such as e-beam and X-ray lithography, proton beam writing (PBW), and AAOs [10–16]. However the AAOs are considered to be the better choice by most material researchers, because of their simple and rapid fabrication and cost effectiveness. In order to study the size dependent behaviors, two anodized alumina membranes were used for growing Fe NWs. One is from Whatman International Ltd. with pore diameter ∼200 nm and thickness ∼60 μm. The other one is homemade, according to the procedure described in [17, 18] with diameter ∼60 nm and thickness ∼80 μm. For the homemade AAO, a commercially available aluminum foil with purity∼99.9995% and initial thickness of 130 μm was employed. First, the pure aluminum foil was mounted on a copper plate, which served as the anode electrode, and was subjected to electro-polishing in a H_3PO_4: H_2SO_4: H_2O solution with weight ratio 4:4:2 for obtaining a clean and smooth surface. After that, a two-step anodization was performed in a 0.3 M oxalic acid solution with a constant potential of 40 V at a temperature around 0–3 °C for two days to form nano-pores. Subsequentially, the product was soaked in $CuCl_2$ and NaOH solutions to remove the remaining aluminum and barrier layers.

In order to perform chemical electro-deposition, a gold layer was deposited on the bottom side of the AAO by means of thermal evaporation to serve as the cathode electrode. Iron was electrodeposited into a porous membrane using dc electrolysis in a solution of $FeSO_4$:$7H_2O$ (0.43 M) and boric acid (0.72 M) with pH∼3 at room temperature. Deposition was carried out with a constant potential at −1.2 V with platinum counter electrodes [19, 20]. The iron was overgrown to form a film layer on the upper surface of the AAO. The shinny iron surface on the membrane indicated that the oxidation of iron was negligible. Finally, a gold electro-deposition was carried out to form a thin layer on the surface of the iron nanowire (Fe NW) arrays. The gold layer plays two roles; it protects the surface of the NWs from oxidation, and serves as the contact layer for the resistance measurement. For the study of the magneto transport properties of the NW arrays, four platinum wires were connected to both sides of the AAO with silver paste. In order to study the magnetization without the influence of electrodes, both sides of the AAO were polished to remove the gold film contacts. After the magnetization measurement, the XRD pattern of the Fe NW arrays was taken immediately, no noticeable oxidation of iron was revealed.

III. RESULTS AND DISCUSSION

The morphology and lattice structure were determined with a scanning electron microscope (SEM, Hitachi S-4200) and X-ray diffraction (XRD, Philips PW3040/60), respectively. The diameter and length of the pores in the AAO were determined by the plane and cross section SEM images, respectively. The diameter and thickness of the Fe NWs are estimated to be ∼60 nm and ∼80 μm, respectively, with a filling factor higher than 70% (the insets of Fig. 1).

The X-ray diffraction was carried out to examine the composition and texture of the

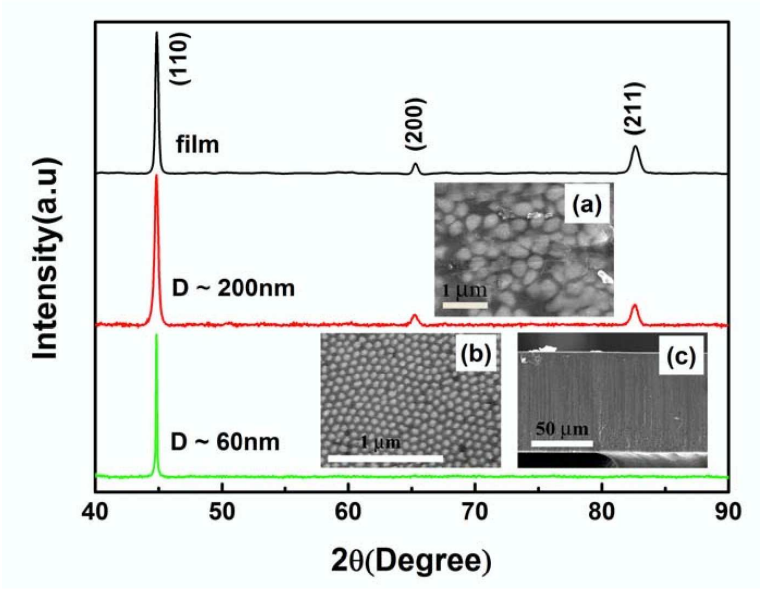

FIG. 1: X-ray diffraction patterns of the film, 200-nm, and 60-nm NWs. Insets (a) and (b) are the cross section view of the 200 and 60 nm NW arrays, respectively. The white spots represent the nano-pores filled with α-Fe phase. (c) is the side view of the home-made empty AAO template.

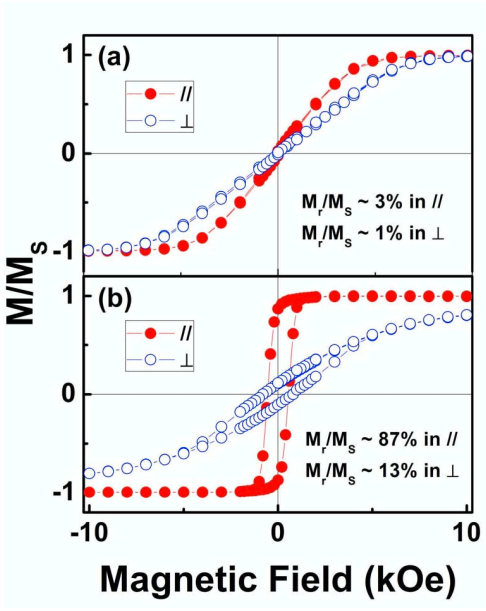

FIG. 2: Hysteresis loops of the NW arrays with magnetic field parallel ($\|$) and perpendicular ($\perp$) to the longitudinal axis of the NWs: (a) 200-nm and (b) 60-nm NWs.

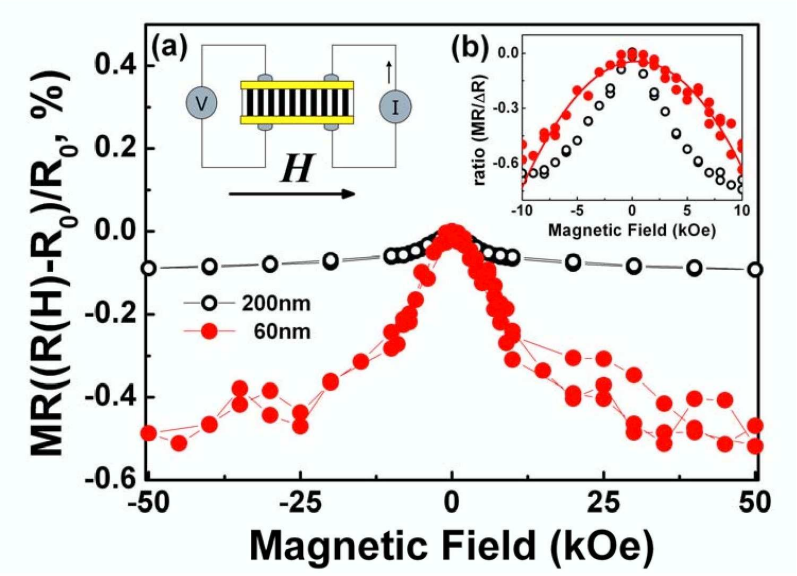

FIG. 3: Magneto-resistance of NW arrays, with the current applied on the longitudinal axis of the Fe NWs and perpendicular to the applied magnetic field. Inset (a): transport measurement setup. The 200 nm gold layers are deposited onto both the top and bottom sides of samples to serve as the electrodes. Inset (b): the normalized $MR/\Delta R$ ratio of the 60 and 200-nm NWs. The parabolic fitting based on Eq. (2) for the 60-nm NWs is represented by the solid line.

NWs (Fig. 1). For the 200 nm Fe NWs the diffraction peaks were identified to be the (110), (200), and (211) planes of α-Fe; the result indicates that the 200 nm Fe NW are a poly-crystal material, whereas the 60 nm Fe NW shows a strong diffraction peak corresponding to the [110], indicating a preferred orientation along the longitudinal axis [11]. At the same time, the NWs were confirmed to be Fe by the element identification of energy-dispersive X-ray analysis (EDX, Hitachi S-4200).

The size effects on magnetism of the Fe NWs were investigated by a Quantum Design Magnetic Property Measurement System (MPMS). The hysteresis loops for the Fe NW arrays at 300 K are shown in Fig. 2. The 60 nm Fe NWs array shows stronger hysteresis and anisotropic behavior, revealed by the larger difference between the magnetization data of the fields parallel and perpendicular to the axis, as compared with that of 200 nm NWs. These results arise from the fact of the magnetic easy axis and preferred crystal orientation of [110] along the longitudinal direction of NWs, which originated from the line shape anisotropy and the large aspect ratios in NWs. The aspect ratios are calculated to be 300 and 1300 for 200 nm and 60 nm, respectively.

As an external perpendicular magnetic field is applied to the 60 and 200 nm NWs, the magnetization was saturated for the 200 nm NWs at a field up to one Tesla, but not for the 60 NWs. The explanation is that for large-diameter NWs, the square ratio and the coercive force decrease appreciably due to the smaller anisotropy and the formation of a multi-

domain structure. Interaction between NWs in dense NW arrays should not be disregarded also, because of the possibility of the appearance (as a result of the interaction) of large demagnetization fields keeping the moments along the longitudinal axis. The hysteresis loops shows that the coercive fields in the easy axis (along the longitudinal direction of NWs) are ∼600 Oe and ∼100 Oe for the 60 nm and 200 nm NWs, respectively. The ratios of the remanence (M_r) to the saturation magnetization (M_S) are about 3% for the 200 nm and 87% for the 60 nm NWs. The magnetization is thus concluded to be more stable in the longitudinal direction of the NWs.

The magneto-transport properties were investigated by the Quantum Design Physical Property Measurement System (PPMS) with the sketch of the measurement setup in the inset Fig. 3(a). The measurement of the magneto-resistance is performed with the applied magnetic field perpendicular to the long axis. In the arrangement the electric current is perpendicular to the applied magnetic field. The calculation of the magnetoresistance (MR) is performed with the formula

$$MR = \frac{R(H) - R_0}{R_0} \times 100\%, \tag{1}$$

where $R(H)$ and R_0 represent the resistance with and without a magnetic field, respectively. The obtained MR curves are mainly attributed to the anisotropic magnetoresistance (AMR) in low-dimensional systems. The AMR is caused by an anisotropic scattering of electrons with strong dependence on the orientation of the external magnetic field relative to the current direction. This consequence originates from the spin-orbit interaction.

The value of the MR ratio of the 60 nm NW arrays is about 5 times higher than that of the 200 nm one at 5 Tesla. This can be attributed to the existence of additional scatterings related to various spin-diffusion mechanisms, which strongly depend on disorder and grain-boundary conditions [21]. The field dependent resistance change due to AMR in the transverse case can be described as [22]

$$R(H) - R_0 = -\Delta R \frac{M_S^2}{4K^2} H^2, \tag{2}$$

where R_0 is the maximum resistance , ΔR is the absolute resistance variation, defined as $|R(5T) - R(0)|$, M_S is the saturation magnetic moment, and K is the shape anisotropy energy constant. The normalized MR ratio ($MR/\Delta R$) is shown in the inset of Fig. 3(b). The data for the 60 nm NWs are better fitted to Equation (2), indicating that the anisotropy constant for the 60 nm NWs is higher than that of the 200 nm NWs.

IV. CONCLUSIONS

In conclusion, two highly ordered Fe NW arrays were prepared by electrochemical deposition and investigated using XRD, EDX, SEM, SQUID, and an electric properties measurement system. The XRD pattern shows a strong texture in the (110) plane along the longitudinal axis of the NWs. The magnetization hystersis loops show a stronger

anisotropic behavior in the 60 nm NW array, which is attributed to its higher aspect ratio. The obtained MR curves are attributed to the anisotropic magnetoresistance AMR. The value of the MR ratio of the 60 nm NWs is higher than that of the 200 nm NWs, which can be attributed to the existence of additional scatterings related to various spin-diffusion mechanisms.

References

[1] D. H. Reich *et al.*, J. App. Phys. **93**, 7275 (2003).
[2] M. Shiraki, Y. Wakui, T. Tokushima, and N. Tsuya, IEEE Trans. Magn. Mag. **21**, 1465 (1985).
[3] L. Sun, Y. Hao, C.-L. Chien, and P. C. Searson, IBM J. Res. Develop. **49**, 79 (2005).
[4] K. Liu, K. Nagodawithana, P. C. Searson, and C. L. Chien, Phys. Rev. B **51**,7381 (1995).
[5] V. Skumryev *et al.*, Nature **423**, 850 (2003).
[6] D. Weller and A. Moser, IEEE Transactions on Magnetics **35**, 4423 (1999).
[7] D. A. Thompson and J. S. Best, IBM J. Res. Develop. **44**, 311 (2000).
[8] T. M. Whitney, J. S. Jiang, P. C. Searson, and C. L. Chien, Science **261**, 1316 (1993).
[9] L. C. Sampaio *et al.*, Phys. Rev. B **61**, 8976 (2000).
[10] D. J. Sellmyer, M. Zheng, and R. Skomski, J. Phys.: Condens. Matter **13**, R433–R460 (2001).
[11] J. B. Wang *et al.*, Nanotechnology **15**, 485–489 (2004).
[12] L. Piraux *et al.* Appl. Phys. Lett. **65**, 2484 (1994).
[13] F. Rousseaux *et al.*, J. Vac. Sci. Technol. B **13**, 2787 (1995).
[14] O. Fruchart *et al.*, Phys. Rev. B **57**, 2596 (1998).
[15] F. Wacquanta *et al.*, J. Appl. Phys. **85**, 5484 (1999).
[16] P. G. Shao, J. A. van Kan, K. Ansari, A. A. Bettiol, and F. Watt, Nuc. Instr. and Meth. Phys. Rsch. B **260**, 79–482 (2007).
[17] S. A. Knaack, M. Redden, and M. Onellion, Am. J. Phys. **72**, 856 (2004).
[18] T. Ohgai *et al.*, J. Phys. D: Appl. Phys. **36**, 3109–3114 (2003).
[19] A. J. Yin, J. Li, W. Jian, A. J. Bennett, and J. M. Xu, Appl. Phys. Lett. **79**, 1040 (2001).
[20] D. AlMawlawi, N. Coombs, and M. Moskovits, J. Appl. Phys. **70**, 4421 (1991).
[21] C. H. Marrows, Adv. in Phys. **54**, 585-713 (2005).
[22] M. Brandsa and G. Dumpich, J. Appl. Phys. **98**, 014309 (2005).